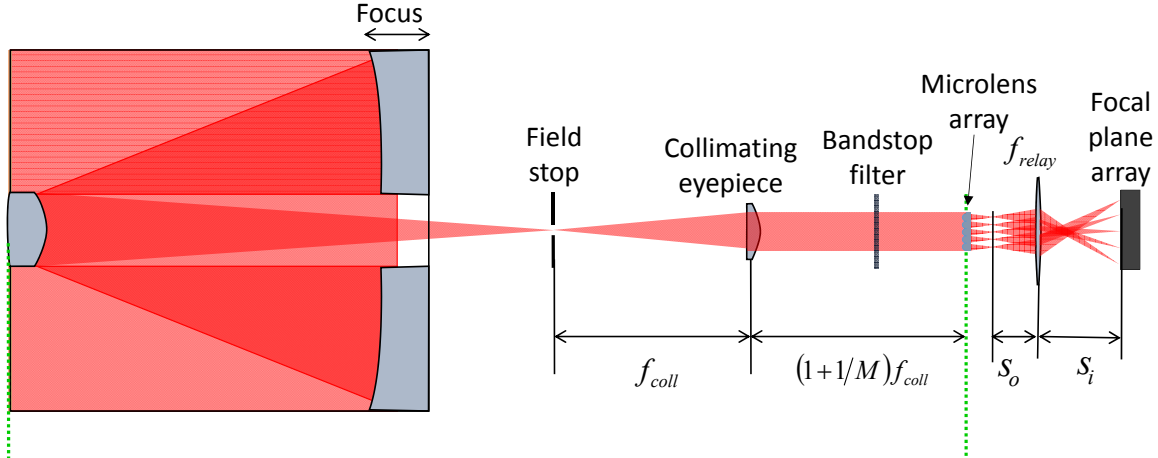


## 3.2 Atmospheric Profiler using Wavefront Sensors and Multiple LED Signals

### 3.2.1 Multi-Color LED Wavefront Sensor Profiler Design and Hardware

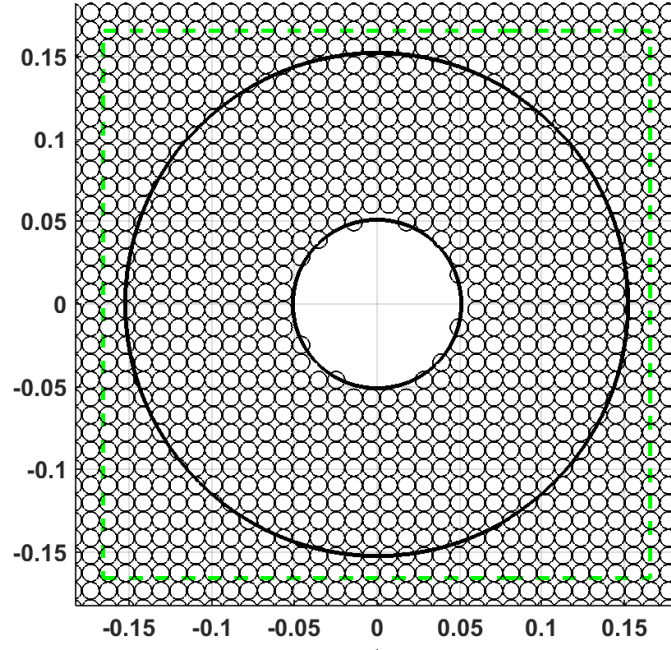
The telescopic color WFS uses the 30.5 cm diameter *Meade f/10* Schmidt-Cassegrain telescope shown at left in Figure 6. This color WFS is nearly the same design as the monochrome telescopic WFS described in previous sections. A schematic of the color WFS is shown in Figure 27. However, this color WFS relies on the Bayer color filter array on the camera’s image sensor to distinguish between red, green, and blue LED sources. This spectral filtering enables simultaneous measurements of wavefront tilts from spatially separated red, green, and blue LEDs.



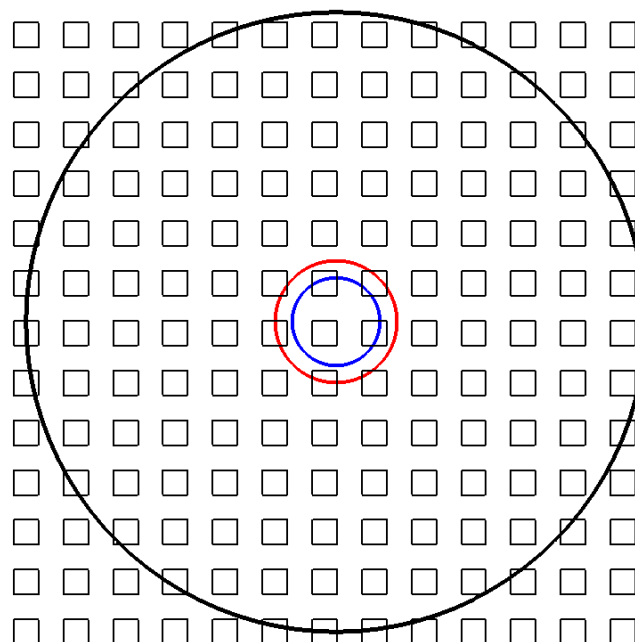
**Figure 27:** Schematic diagram of the telescopic color WFS. Light from the distant LEDs enters the 30.5 cm diameter Schmidt-Cassegrain telescope from the left. An iris placed at telescope’s prime focus serves as a field stop to reduce background light. An eyepiece collimates the light, and a bandstop filter further reduces non-LED light. A microlens array is placed in a plane conjugate to the telescope entrance pupil and a relay lens reimages the microlens spots with possible magnification onto the color focal plane array.

The telescopic color WFS was designed to have approximately 1 cm diameter subapertures which provides good quality spot images over a wide range of turbulence conditions. Since the color WFS must operate from blue to red wavelengths, the collimation and relay optics were selected to minimize chromatic aberrations. The effective pixel sampling of microlens spot images was designed to provide the adequate spatial sampling and signal-to-noise ratio (SNR) performance required for accurate centroid measurements. The number of pixels per subaperture was selected to balance tilt measurement dynamic range with acquisition frame rate. Figure 28 shows the WFS subapertures within the telescope entrance pupil on the left and the effective pixel sampling across a single subaperture on the right. The subapertures are 1.03 cm in diameter, and the pixel angular IFOV is 24.7 microradians in output space. During initial field tests, we achieved 167 frames-per-second image acquisition using the 800-by-800 pixel resolution indicated by the dashed green square shown at left in Figure 28. With the camera region of interest reduced to 730-by-730 pixels just covering the active subapertures, we expect to achieve a 200 frames-per-second image acquisition rate.

We selected a *Point Grey Grasshopper3, GS3-PGE23S6C-C* color GigE CMOS camera based primarily on its resolution, frame rate, and Bayer color filter array spectral response. Good spectral separation between LED source wavelengths is critical for accurate wavefront tilt measurements. Figure 29 shows the published spectral response of the *Sony IMX-174* image sensor used by the *Grasshopper3*



(a)



(b)

**Figure 28:** The 30.5 cm diameter color WFS entrance pupil showing the 1.03 cm subapertures with an 800-by-800 focal plane array superimposed (left). The pixel sampling behind a single subaperture with  $\lambda/D$  diameter spots for the red and blue LED wavelengths superimposed (right). Note, the 25% pixel area fill factor that results from decimation of the Bayer color filtered image. With this WFS configuration, we achieved 167 fps acquisition rates and 24.7 microradian angular IFOV.

with the measured emission spectra of our red and blue LED transmitters superimposed. Ideally, the red, green, and blue pixels should respond to only the red, green, and blue LEDs respectively without crosstalk. Spectral crosstalk results in wavefront tilt measurement errors and would likely be difficult to remove post-detection. We observe that the camera's published red pixel response is roughly  $30\times$  that of the blue pixel response at the red LED wavelength. Similarly, we observe that the camera's published blue pixel response is roughly  $20\times$  that of the red pixel response to the blue LED wavelength. Illuminating the image sensor with only the red LED transmitter in a darkened lab, we measured approximately a 35:1 red to blue pixel response which is slightly better than expected. Similarly, when illuminating the image sensor with only the blue LED transmitter, we measured approximately a 24:1 blue to red pixel response which is also slightly better than expected. The lab test confirms that the *Sony IMX-174* color filter array exhibits good red and blue spectral separation.

However, the green wavelength is problematic. We observe that in order to minimize spectral crosstalk, a green/yellow LED source must selected which emits at approximately 575 nm. We are not aware of the existence of high power LEDs which emit at these wavelengths, except for wide band LEDs that rely on fluorescence. Such a fluorescent LED can be filtered so that it only emits in the desired 575 nm window, but with a considerable reduction in optical power. Additionally, the color camera's green filter response shows considerable overlap at the red LED emission wavelengths introducing possible crosstalk noise.

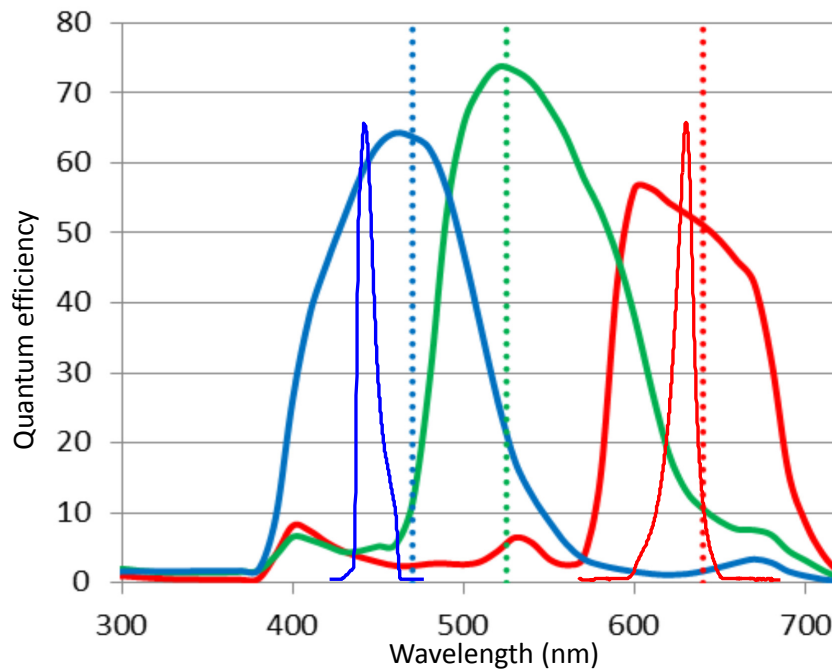


**Figure 29:** Published *Sony IMX-174* image sensor spectral response with measured red and blue LED emission spectra superimposed.

Initial field tests were conducted using red, green, and blue LED transmitters. A raw 800-by-800 pixel resolution color WFS image is shown at top in Figure 30 which is then decimated into the 400-by-400 pixel resolution red, green, and blue images shown at the bottom of Figure 30. The field test confirmed the limitations associated with the green wavelength. First, with the green LED operating at maximum power and the red and blue LEDs operating near minimum power, the received green power was less than the either the red or blue so that the green LED ultimately limits the range at which the color WFS can operate. Second, red/green crosstalk is evident in Figure 30 in which the green pixels show considerable response to the red LED.

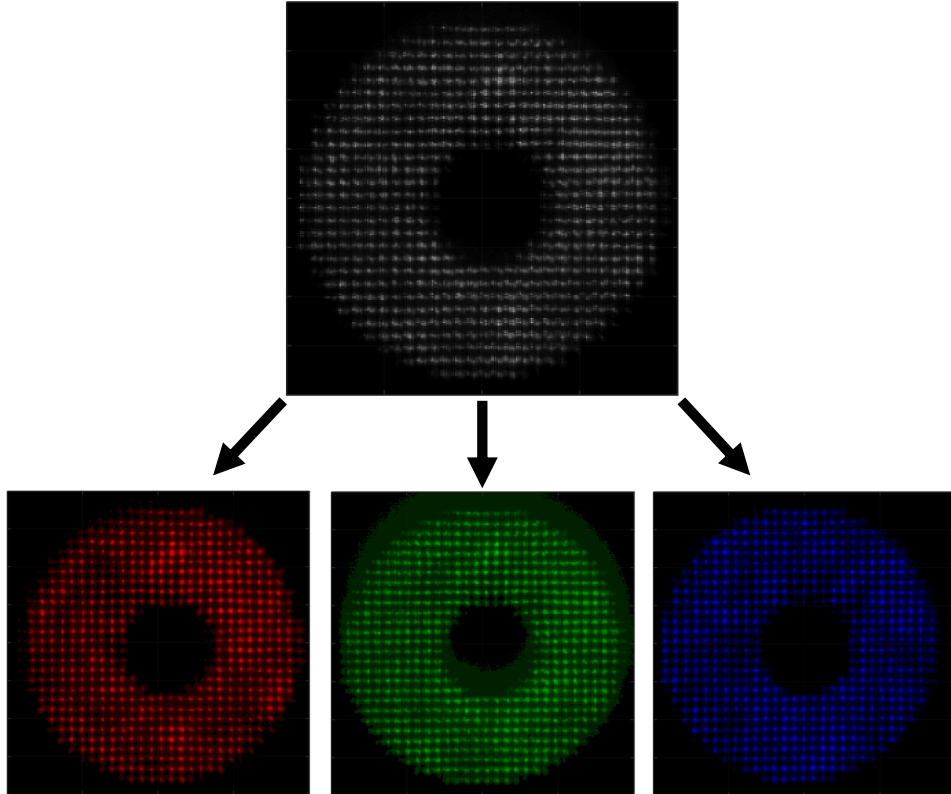


**Figure 30:** Raw 800-by-800 pixel resolution color WFS image decimated into 400-by-400 pixel resolution, red, green, green, and blue images. (Only one of the two green images is shown). Note the double spots visible in the green image - spots which coincide with the spots in the red image.

The color WFS is capable of distinguishing between spatially separated red, green, and blue LEDs. However, narrowband green LEDs with optical irradiance comparable to that of red and blue LEDs are not currently commercially available. Additionally, the Bayer color filter array on most cameras show significant spectral overlap between the green and blue wavelengths and the green and red wavelengths. Because of these green wavelength drawbacks, we showed in the previous report that a color WFS operating with just spatially separated red and blue LEDs can measure differential tilts with many unique path weights that can effectively estimate  $C_n^2$  atmospheric turbulence profiles. Therefore, we optimized the design of the color WFS for operation at red and blue LED wavelengths. The color WFS employs a magenta bandpass filter to pass the red and blue LED sources and reject a large portion of the background radiance. In order to minimize spectral crosstalk, we also built new transmitter modules using red and blue LEDs with narrow emission spectrums matched to the specific color filter array present on the WFS camera. We measured the camera's normalized red pixel response to the

new blue LED at 3.2% and the normalized blue pixel response to the new red LED at 2.4%. These are both 20% reductions in spectral crosstalk from the previous version of the transmitter module.

Each of the new transmitter modules is affixed to a dovetail carrier that mates with a dovetail rail attached to the WFS's optical tube assembly . For double-ended WFS measurements, the LED transmitter modules should be boresighted with the color WFS's optical tube assembly. The dovetail system allows the transmitter module to be easily removed for transport and precisely reinstalled for repeatability accurate boresighting. Photographs of a complete color WFS with the new transmitter module are shown in Figure 31.



**Figure 31:** 30.5 cm diameter color WFS transmitting green, blue, and red eyesafe LEDs (left). Rear view of the same color WFS with the optical train visible (right).

### 3.2.2 Wave-Optics Simulation of the Wavefront Sensor Profiler

We conducted a wave-optics simulation of a color WFS-based turbulence profiler that uses two color LED transmitters. The turbulence profiler modeled in the simulation was very similar in construction to the as-built turbulence profiler field tested during this reporting period. The wave-optics simulation verified the ability of the two color WFS-based turbulence profiler to measure range resolved  $C_n^2$ .

In the wave-optics simulation, the user first inputs the  $C_n^2$  turbulence strength along the propagation path. The simulation outputs WFS subaperture tilt time histories. Differential tilt variances are then computed for specific transmitter/receiver geometries available within the WFS pupil. Because

theoretical differential tilt path weight functions can be computed for each transmitter/receiver geometry, a range resolved  $C_n^2$  profile can be estimated using an stochastic parallel gradient descent (SPGD) matrix inversion. Since a known  $C_n^2$  turbulence profile is input to the wave-optics simulation, a direct comparison to the output  $C_n^2$  profile is possible. The 20 (10 from each side) theoretical path weights of the transmitter/receiver geometries used in the simulation are shown in the left plot in Figure 32. The results of the wave-optics simulation using a slightly asymmetric input  $C_n^2$  profile are shown by the red plot at the right in Figure 32. The theoretical path weights and differential tilt measurements from the simulation were fed into an SPGD algorithm to estimate the  $C_n^2$  profile shown by the black plotted line. The SPGD inversion was performed 15 times resulting in the standard deviation bounds shown by the blue plotted line. From the simulation results, we observe that the two-color WFS system measures a  $C_n^2$  profile with the correct shape, but slightly underestimates the turbulence strength at all ten range bins. This is a phenomenon previously observed in simulations of MZA's existing atmospheric turbulence profiler product. In fact, the existing turbulence profiler applies a small correction factor to account for this underestimation.

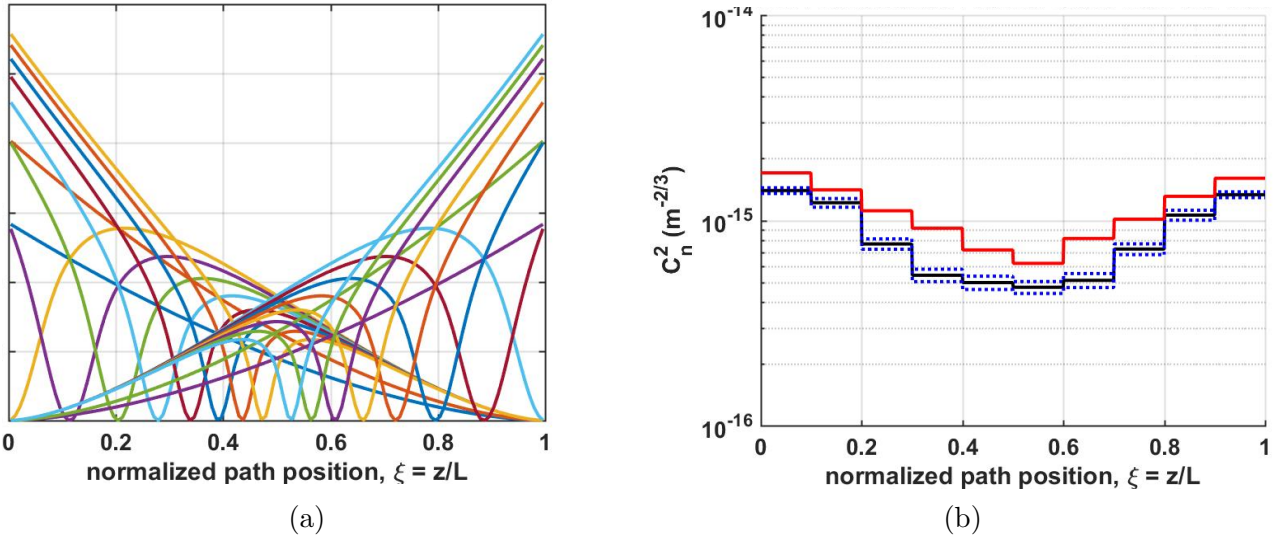


**Figure 32:** Wave-optics simulation of a color WFS-based profiler. The 20 differential tilt path weight functions exploited by the simulated color WFS-based profiler (a). The input (red) and estimated (black)  $C_n^2$  profiles from the simulation. 15 realizations of the SPGD algorithm were run generating 15 estimated profiles whose standard deviation is shown by the dotted blue lines.

The transmitter/receiver geometries used in the aforementioned simulation were limited to single subaperture receivers, though subaperture ganging is possible with the  $C_n^2$  estimation software. During a study of transmitter/receiver geometries that might form an effective basis for  $C_n^2$  estimation, we noted that differential tilt variances between closely spaced receiver subapertures measured from the simulation were consistently lower than theoretical differential tilt predictions. Figure 33 shows the results of a study in which the atmospheric coherence diameter,  $r_0$  is estimated from the differential tilt measured between a pair of subapertures. We observe that  $r_0$  measured from the wave-optics simulation data is about 14% higher than theoretical predictions for widely spaced subapertures. MZA has observed this behavior in previous profiler simulations. In fact, the green line plotted in Figure 33 shows the approximately 14.5% correction factor MZA applies to  $r_0$  measurements made by previous version of the atmospheric turbulence profiler. However, as the receiver spacing decreases below four subapertures, we also observe an increasing overestimation of  $r_0$ , up to approximately 27% for adjacent subapertures. This is a new discovery and may warrant further investigation.

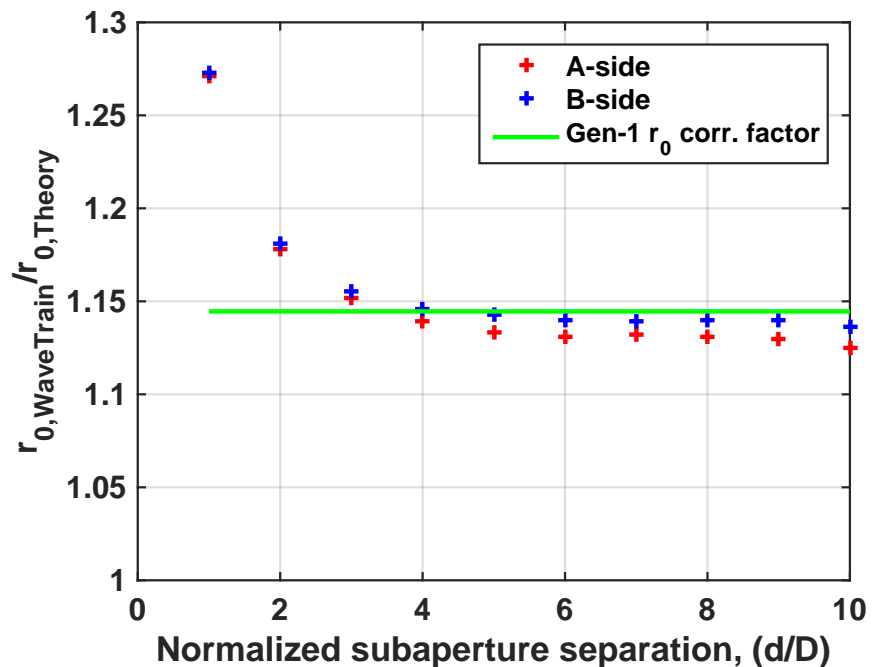


Figure 33: Comparison of the atmospheric coherence diameter,  $r_0$ , computed from differential tilt measurements of the wave-optics simulated color WFS and computed theoretically from the known  $C_n^2$  profile. The green line shows the approximately 14.5% correction factor MZA applies to the  $r_0$  measurements made by the first generation atmospheric turbulence profiler.